http://dx.doi.org/10.21611/qirt.2014.192

Non-intrusive thermal measurement methods adapted to painted cave walls

by E. Legloanec*, A. Sommier*, A. Sempey*, P. Malaurent, D. Lacanette*, JC. Batsale*

* Univ Bordeaux, I2M, CNRS, UMR 5295, F-33400 Talence, France.
CNRS, I2M, UMR 5295, F-33400 Talence, France.
Arts et Metiers ParisTech, I2M, UMR 5295, F-33400 Talence, France.
a.sempey@*i2m.u-bordeaux1.fr*

Abstract

Painted caves such as Lascaux are highly sensitive to their surrounding atmospheric conditions. To preserve them for the upcoming generations, it is necessary to understand thermal and mass transfers that happened between the painted walls and the air. A cave has been monitored with an infrared camera and a Peltier sensor. The singular value decomposition has been first applied to extract the relevant information. It revealed a non-random thermal behavior of the wall. Then a semi-infinite model combined with a Fourier analysis led us to evaluate the thermal effusivity of the cave wall. This latter is subjected to large measurement uncertainties.

1. Introduction

Caves are a complex environment. Their inner average temperature remains almost constant during the whole year and they present a very high humidity rate, close to 100%. Due to the daily outside temperature variations, an air circulation is created between the bottom of the cavity and the outside (the reversed process happens as well, depending on both the temperatures of the cavity end and the outside). Some of those cavities, such as Lascaux (Dordogne, France), are subject to a high level of interest because of their painted walls: they represent a proof of our ancestors' way of living. At the same time, those works of art are very sensitive to their surrounding environment. For example, the simple presence of a person on site can slightly unbalance the thermal equilibrium of the cavity. This perturbation, as negligible as it seems to be, could have dramatic and irreversible consequences on the shape of those paintings.

A lot of efforts have been dedicated for years to the preservation of those works of art. This brings about the thorough understanding of how the air cavity interacts with the paintings. It also means specific measurements have to be set up and this is where it gets complex. Therefore this paper discusses the possibility of using the infrared thermography as a way of conducting in situ measurements. Indeed, this technique presents the advantage of being a non destructive method: it means measures can be carried out without any physical contacts with the studied surface. This technique has already been implemented to the conservation of historical monuments [1,2,3], especially by detecting the presence of humid zones at different locations on the building walls. Humidity rates are crucial to know because they are one of the mediums of moisture spreading, which is an indicator of the building shape.

Rather than using a whole set of infrared images, only a couple of them are often analyzed. Therefore, multiple information like a time behavior after a thermal perturbation is put aside. In 2012, Dumoulin et al. [4] explained how they studied an Italian bridge during three days. The set of infrared images revealed interesting inner characteristics after being computerized. Those different works, related to the preservation of multiple kinds of buildings, inspired us to apply thermographic studies to cavities.

This paper aims at adapting non-intrusive thermal measurement methods to painted cave walls. The method proposed combines the singular value decomposition (SVD) and the Fourier decomposition in order to analyse a set of infrared images. Results are used in order to estimate the effusivity of the wall in taking into account the uncertainties in taking into account the uncertainties. The experimental site and the measuring devices are presented in section 2. Sections 3 and 4 are devoted to the analysis of measures with respectively the Singular Value Decomposition and the Fourier decomposition. Last section includes a description of the semi-infinite wall model used to determine the thermal effusivity of the wall.

http://dx.doi.org/10.21611/qirt.2014.192

2. Measurements realization

Those phenomena were observed inside a cavity which doesn't present any historical concerns. In other words, it is only used for scientific purposes. This place is located in Dordogne (France), on the township of "Les Eyzies de Tayac Sireuil". Only the entrance to cavity was studied (figure 1). Since this part is close to the surface, it is still influenced by the daily temperature variations compared to the bottom of the cavity.

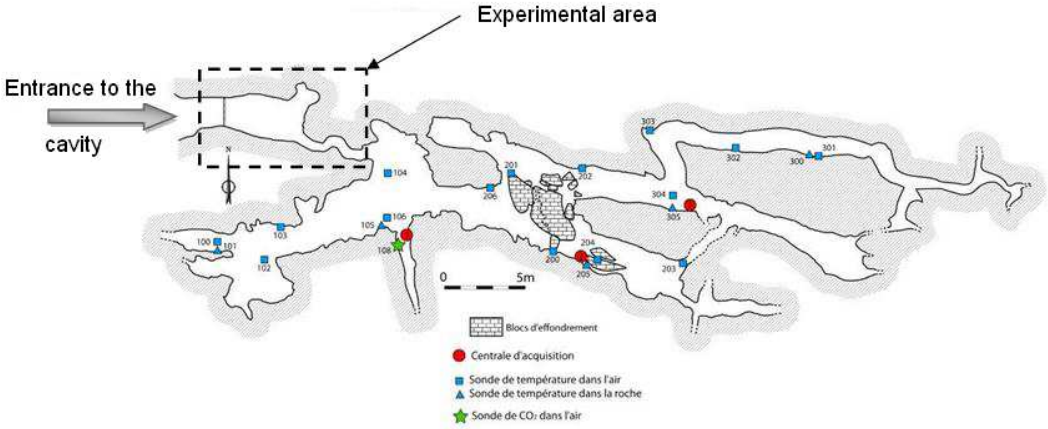

Fig. 1. *Cavity plan*

The set up included various sensors (temperature, humidity, heat flux) and an infrared camera. The Peltier sensor was in the field of view of the infrared camera (figure 2) which recorded a picture of it each ten minutes during an entire week. Five temperature sensors and three humidity sensors were installed on a measurement bar in order to properly monitor the temperature gradient which is established from the floor to the ceiling of the cave corridor. This is due to the temperature difference between the outside and the bottom of the cavity since heat moves from warm to cold parts: depending on those two temperatures, a permanent air movement occurs between the outside and the bottom of the cavity. Since warm air has a lower density compared to cold air, it moves at the upper part of the corridor. Those air movements, combined with high humidity rates, are likely to generate vaporization and condensation phenomena at the surface of the rock where the Peltier sensor is set up.

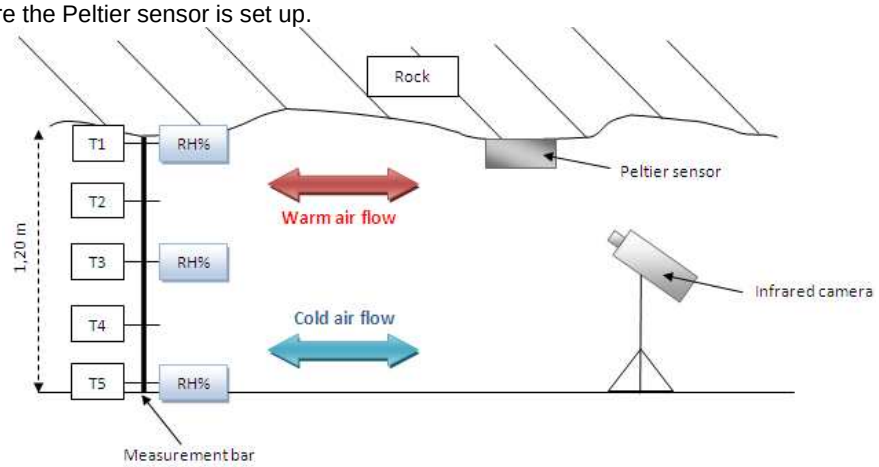

Fig. 2. *Material disposition*

http://dx.doi.org/10.21611/qirt.2014.192

3. Singular value decomposition analysis

The experience took place during a week: it recorded almost one thousand thermograms. The first idea to interpret them would be to look at the whole set of picture one by one. This technique did not show any characteristic behaviors because the phenomena we were looking at had very low magnitude variations. So it made them hard to be visually detected.

Therefore, the singular value decomposition was implemented as a statistic method in order to extract the relevant information from the infrared images. This method is based on the decomposition of an initial matrix A into three others by following the below definition [5]:

$$A = U \times S \times V^t \tag{1}$$

For a physical parameter which depends both in space and time, the former definition can be written again by:

$$\mathrm{A}(\mathrm{x},\mathrm{t}) = \sum_{\mathrm{k}} \mathrm{u_k}(\mathrm{x}) \times \mathrm{S_k} \times \mathrm{v_k}(\mathrm{t}) \tag{2}$$

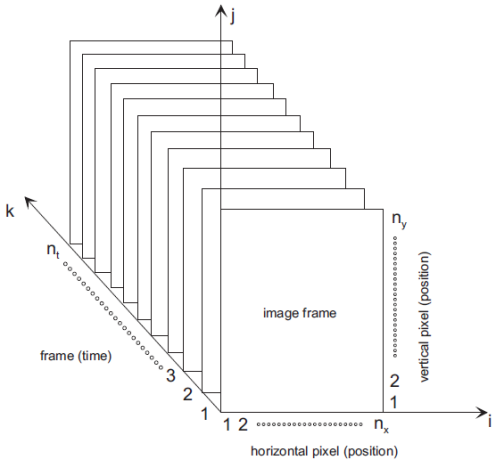

Fig. 3. *Data set of infrared images*

U is an orthogonal matrix, as well as V. Regarding S, this is a pseudo-diagonal matrix. In our case, the matrix A represents the entire set of infrared images, that is to say a physical parameter which depends on both time and space as illustrated through the figure 3. The SVD algorithm is used to reduce the matrix A to a compact statistical representation of the spatial and temporal variations. The columns of the matrix U contain the orthogonal modes describing the spatial variations of the original data. The contributions of those modes vary in time according to the associated matrix V [6]. The matrix S contains the singular values of A on its diagonal; they are stored in a decreased order. Deciding the number of modes to be kept requires looking at the singular values themselves. Most of the time, the first three to five modes account for more than 99 % of the total data variance. This is an important diminution of the original thermographic data set which often contains hundreds of thermograms. In our case, the first two modes account for more than 99 % of the total data. The following pictures (from figure 4 to figure 9) illustrate those two modes: the matrices on the left represent the orthogonal modes U, associated with their respective time variations V on the right.

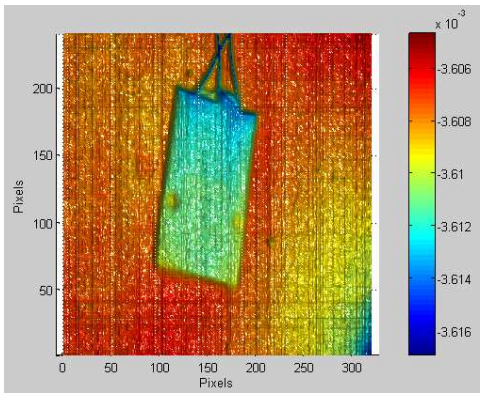

Fig 4. *Representation of U1*

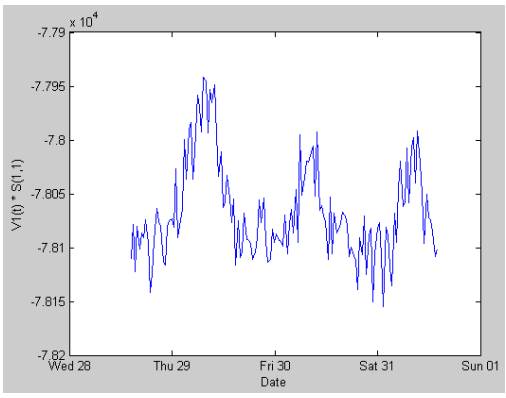

Fig. 5.*Representation of V1 x S1*

http://dx.doi.org/10.21611/qirt.2014.192

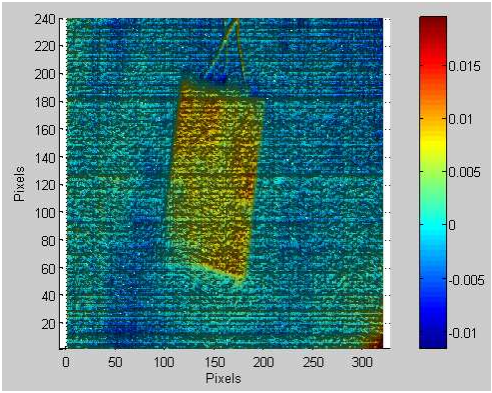

Fig. 6 *.Representation of U2*

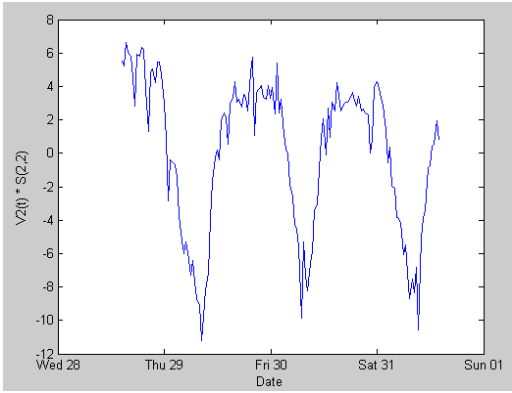

Fig. 7. *Representation of V2 x S2*

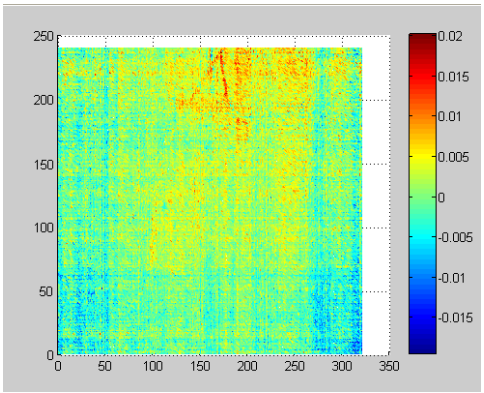

Fig. 8. *Representation of U3*

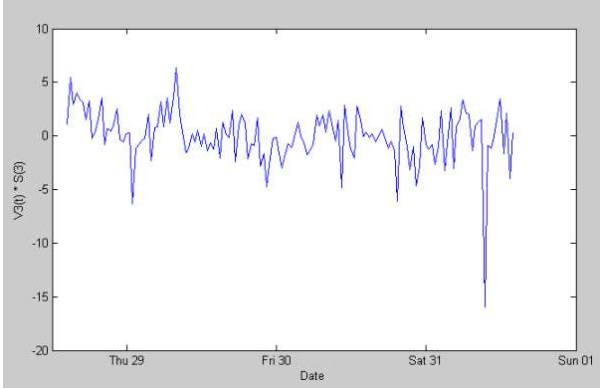

Fig. 9. *Representation of V3 x S3*

This first mode represents the global dynamic behavior of the data set. Regarding the second mode and its temporal evolution, they are fluctuating around zero. This means the second mode is a correction of the global dynamic behavior. The SVD method showed a characteristic behavior of the wall shooted by the infrared camera: it is clear by looking at the temporal responses this behavior is not a random one but a periodic one. Besides, we can notice a difference of behaviour between the Peltier sensor and the wall where it is attached. Regarding the first mode, the wall presents a slightly stronger reactivity to the excitation introduced by the temporal dynamic V1(t). The second mode puts in evidence an opposite second order dynamic between the Peltier sensor and the wall. Indeed, the sign of U2 is different between both these zones. Last, the third mode cannot allow to distinguish the wall and the Peltier sensor. Its dynamic has not any significant meaning. Thus, only the two first modes have a periodic dynamic.

4. The Fourier decomposition

The Fourier decomposition has to be applied to a temporal signal. So for the temperature, a mean value (figure 11) has been computed at each time step for a region of pixel (Figure 10).

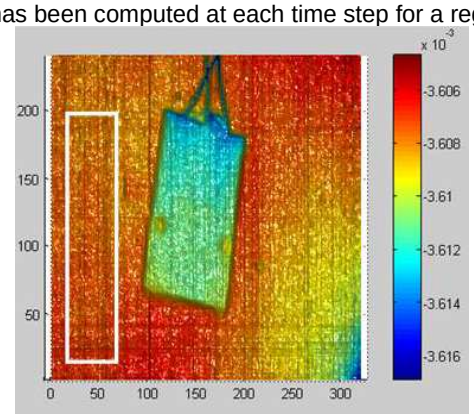

Fig 10. *Pixel zone for the mean temperature*

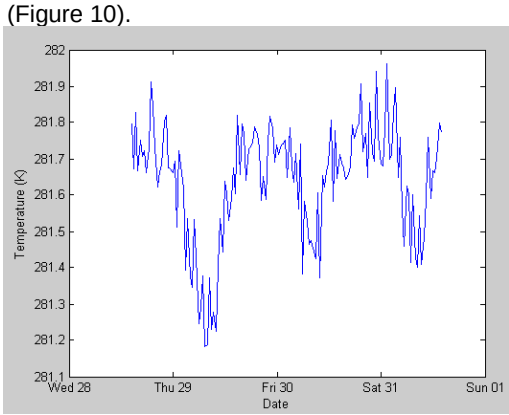

Fig. 11.*Temperature of the pixel zone*

http://dx.doi.org/10.21611/qirt.2014.192

A frequency spectrum of the heat flux and temperature signals, V1(t) and V2(t) has been computed. The figures 12 to 19 show the frequency spectrum for the left ones and their respective power spectral densities (also known as PSD) for the right ones.

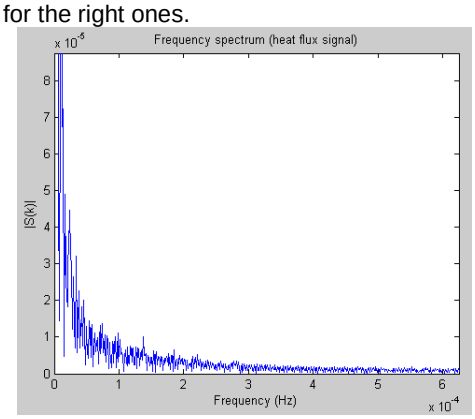

Fig. 12. Heat flux Fourier transform

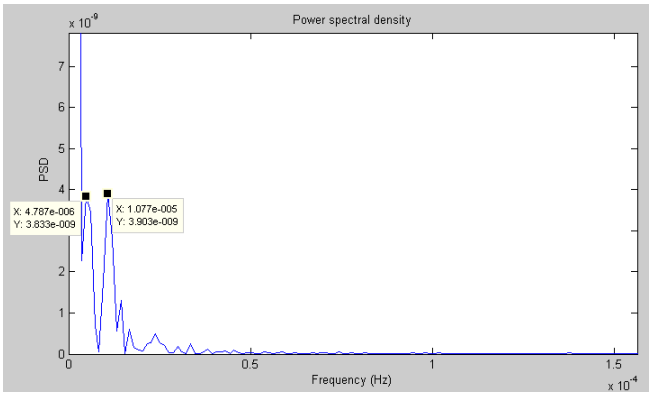

Fig. 13. Heat flux PSD

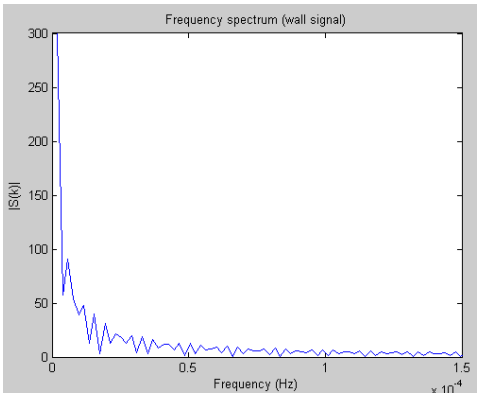

Fig. 14. Wall temperature Fourier transform

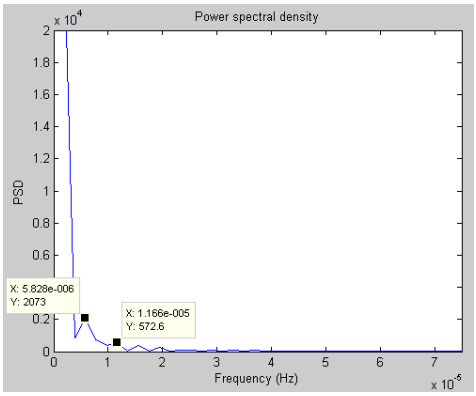

Fig. 15. Wall temperature PSD

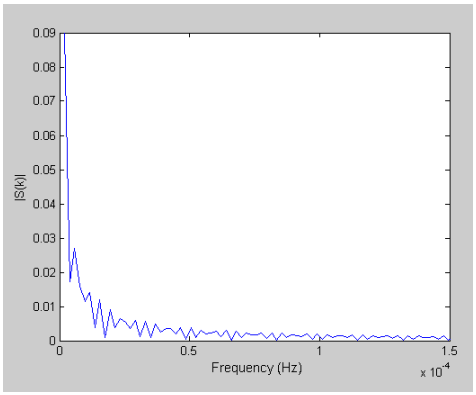

Fig. 16. *V1(t) Fourier transform*

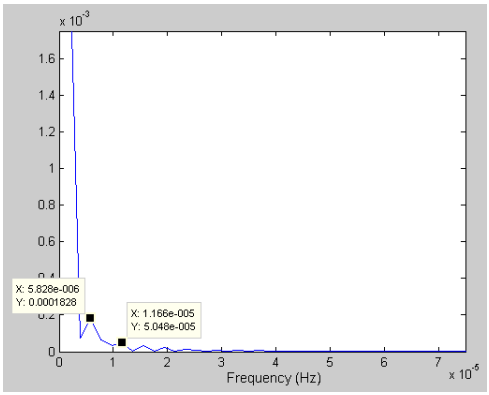

Fig. 17. *V1(t) PSD*

http://dx.doi.org/10.21611/qirt.2014.192

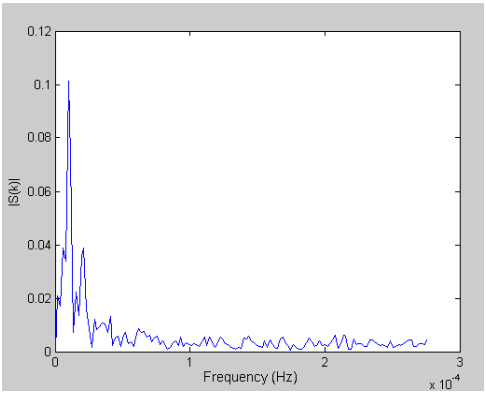

Fig. 18. *V2(t) Fourier transform*

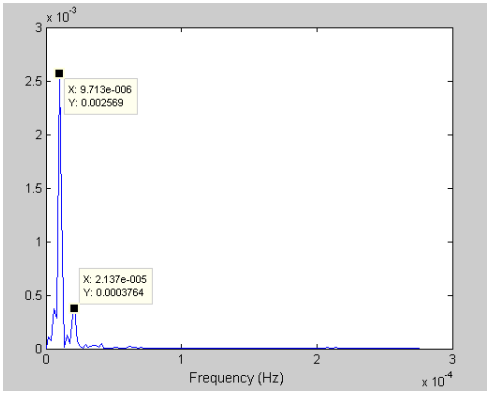

Fig. 19. *V2(t) PSD*

The characteristic frequencies identified on those two signals are presented through the table 1.

Table 1. *Characteristic frequencies*

Signal	Characteristic frequency	Characteristic period
Heat flux	4.787×10^{-6} Hz	208 899 s
	1.074×10^{-5} Hz	93 110 s
Wall temperature	5.828×10^{-6} Hz	171 585 s
	1.166×10^{-5} Hz	85 763 s
V1(t)	5.828×10^{-6} Hz	171 585 s
	1.166×10^{-5} Hz	85 763 s
V2(t)	9.713×10^{-6} Hz	102 955 s
	2.137×10^{-5} Hz	46 795 s

At first, we can notice that the wall temperature and V1(t) have exactly the same characteristics. This fact can be explained by the remembering that the first mode of the SVD analysis contains more than 99% of the total data. For the the heat flux and wall temperature signals the characteristic periods are not exactly the same but they both correspond to a time variation of approximately two days for the first one and approximately one day for the second one (an entire day has 86 400 seconds). This means a phase lag calculation can be implemented regarding those two signals at those two identified frequencies. The Fourier decomposition was used to realize it. Indeed, it specifies a periodical function can be written as a sum of sine and cosine functions, as explained by the following equation [7].

$$f(t) = \frac{1}{t_p} \sum_{n=-\infty}^{+\infty} \tau_n(\omega_n) \exp(i\omega_n t) \tag{3}$$

By considering only the first harmonic of the Fourier decomposition, applied to each of the two signals, we can write the following :

$$Fl_1(t) = \frac{2}{\tau_1} \times A_1(\omega_1) \times \sin\left(\frac{2\pi t}{\tau_1}\right) \tag{4}$$

$$T_1(t) = \frac{2}{\tau_1} \times B_1(\omega_1) \times \cos\left(\frac{2\pi t}{\tau_1}\right) + \frac{2}{\tau_1} \times C_1(\omega_1) \times \sin\left(\frac{2\pi t}{\tau_1}\right) \tag{5}$$

Fl_1 refers to the first harmonic of the heat flux signal and T_1 refers to the first harmonic of the wall temperature signal (recorded by the camera). The different coefficients are expressed by the Fourier's theory:

$$A_1(\omega_1) = \int_0^{\tau_1} Fl_{\text{real signal}}(t) \sin\left(\frac{2\pi t}{\tau_1}\right) dt \tag{6}$$

$$B_1(\omega_1) = \int_0^{\tau_1} T_{\text{real signal}}(t) \cos\left(\frac{2\pi t}{\tau_1}\right) dt \tag{7}$$

$$C_1(\omega_1) = \int_0^{\tau_1} T_{\text{real signal}}(t) \sin\left(\frac{2\pi t}{\tau_1}\right) dt \tag{8}$$

http://dx.doi.org/10.21611/qirt.2014.192

Calculating the previous integrals allowed us to determine and plot the first harmonics of the two studied signals: this is what the figure 20 expresses.

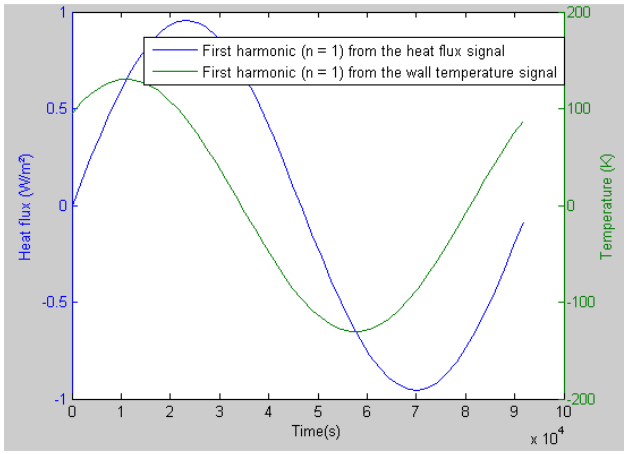

Fig. 20. *First harmonic reconstruction*

The two curves present a phase lag of 42°, which is really close to the characteristic 45° of a semi-i nfinite model. This means the cavity wall we examined can be reasonably assimilated to the semi-infinite model. However, this is only true for the two frequencies identified since this characteristic phase lag was determined only for those two frequencies.

5. The semi-infinite wall model

The previous analysis showed that the behavior of the wall is not a random one. We chose to confront it to mathematical models that are able to describe how a wall reacts to a heat flux excitation. Since cave walls are much thicker than the other characteristic parameters, the semi-infinite wall model appeared to correctly match this consideration.

It gives a relation between the heat flux variations $\Phi(0,\omega_n)$ at the surface of the wall and the temperature variations $\tau_n(0,\omega_n)$ also taken at the surface: this is what stands the following equation [7].

$$\left\|\Phi(0,\omega_n)\right\| = \sqrt{\lambda\rho c}\times\sqrt{\omega_n}\times\left\|\tau_n(0,\omega_n)\right\| \tag{9}$$

It is interesting to notice this equation introduce a phase angle of π/4 between the heat flux and the temperature: this is one of the characteristics of this model. Calculating a phase lag between two physical parameters implies they both have the same frequency. This is not the case here because the two signals we are studied came from in situ measurements. It means each one is composed of many frequencies since they are not theoretical signals.

Since the semi-infinite model is partially valid, the equation which describes it can be used. In terms of norm, this equation can be written as following:

$$E = \sqrt{\lambda\rho c} = \frac{\left\|\Phi(0,\omega_n)\right\|}{\sqrt{\omega_n}\times\left\|\tau_n(0,\omega_n)\right\|} \tag{10}$$

The term $E = \sqrt{\lambda\rho c}$ is the thermal effusivity of the material. It can be evaluated by computing the magnitude of both the surface heat flux and the surface temperature. There are two frequency values, therefore we obtained two values for the wall effusivity (see table 2), which are actually the effusivity of a stone material.

http://dx.doi.org/10.21611/qirt.2014.192

Table 2. *Computed effusivities*

Characteristic period	Corresponding effusivity
τ1 = 93 110 seconds	E1 = 491 $J.K^{-1}.m^{-2}.s^{-1/2}$
τ2 = 208 899 seconds	E2 = 735 $J.K^{-1}.m^{-2}.s^{-1/2}$

Those values are a little smaller than regular stone effusivities. Typically, for regular sandstone, the effusivity is about 1938 $J.K^{-1}.m^{-2}.s^{-1/2}$ with a thermal conductivity of 2.3 $W.m^{-1}.K^{-1}$, a density of 2300 $kg.m^{-3}$ and a specific heat of 710 $J.kg^{-1}.K^{-1}$.
Our calculations are based on wall temperature variations recorded by the infrared camera and on heat flux variations recorded by the Peltier sensor. Those signals had extremely small magnitudes which means even a weak disturbance will have a strong impact on the final effusivity calculation. By taking into account those measurement uncertainties and implementing them into our effusivity calculations, the following range values were obtained:

$$115\ J.K^{-1}.m^{-2}.s^{-1/2} \le E_1 \le 1432\ J.K^{-1}.m^{-2}.s^{-1/2}$$
$$171\ J.K^{-1}.m^{-2}.s^{-1/2} \le E_2 \le 2145\ J.K^{-1}.m^{-2}.s^{-1/2}$$

Such values are now closer to regular rock material effusivities which raises the importance of the measurements uncertainties.

6. Conclusion

Using the infrared thermography to study cave wall behaviors toward thermal excitations revealed interesting characteristics. Indeed, even if the magnitude variations of the signals were really small, they were large enough to be detected by the infrared camera, associated with sensor measurements. At the moment of starting this project, we were not able to decide whether or not applying the infrared thermography to cave wall studies would be a relevant work. Finally, it ended up finding the thermal effusivity of the studied wall. Since it is subjected to large uncertainties, this project would be favorably completed by another study, using a different approach and aiming at increasing the result accuracies. The combination of the SVD and Fourier analysis could be an interesting track. Indeed, the SVD seems to show interesting capacities to extract major information before applying the Fourier transform to the signal.

REFERENCES

[1] E. Grinzato, P. G. Bison, and S. Marinetti, "Monitoring of ancient buildings by the thermal method". Journal of Cultural Heritage, vol. 3(1), pp. 21‑29, 2002.
[2] S. Lagüela, M. Solla, J. Armesto, H. González-Jorge, and C. L. M. Vigo, "Comparison of Infrared Thermography with Ground-Penetrating Radar for the Non-Destructive Evaluation of Historic Masonry Bridges", Proceedings of 11st Quantitative InfraRed Thermography conference, paper QIRT2012-179, Naples (Italy), 2012.
[3] P. Bison, G. Cadelano, and E. Grinzato, "Thermographic Signal Reconstruction with periodic temperature variation applied to moisture classification", QIRT Journal, vol. 8(2), pp. 221‑238, 2011.
[4] J. Dumoulin and R. Averty, "Development of an infrared system coupled with a weather station for real time atmospheric corrections using GPU computing: Application to bridge monitoring", Proceedings of 11st Quantitative InfraRed Thermography conference, paper QIRT2012-224, Naples (Italy), 2012.
[5] M. A. Omar, R. Parvataneni and Y. Zhou, "A combined approach of self referencing and Principle Component Thermography for transient, steady ans selective heating scenarios', Infrared Physics & Technology, vol. 53 (5), pp. 358-362, 2010
[6] N. Rajic, "Principal Component Thermography",DSTO Aeronautical and MAritime Research Laboratory, avr. 2002.
[7] D. Maillet, S. André, J. C. Batsale, A. Degiovanni, C. Moyne," Thermal Quadrupoles: Solving the Heat Equation through Integral Transforms". Wiley ad., 2000.